ADVANCED MATERIALS

Supporting Information

for *Adv. Mater.*, DOI: 10.1002/adma.202007497

A Patternable and In Situ Formed Polymeric Zinc Blanket for a Reversible Zinc Anode in a Skin-Mountable Microbattery

Minshen Zhu, Junping Hu, Qiongqiong Lu, Haiyun Dong, Dmitriy D. Karnaushenko, Christian Becker, Daniil Karnaushenko, Yang Li, Hongmei Tang, Zhe Qu, Jin Ge, and Oliver G. Schmidt*

Supporting Information

A Patternable and In Situ Formed Polymeric Zinc Blanket for a Reversible Zinc Anode in a Skin-Mountable Microbattery

Minshen Zhu, Junping Hu, Qiongqiong Lu, Haiyun Dong, Dmitriy D. Karnaushenko, Christian Becker, Daniil Karnaushenko, Yang Li, Hongmei Tang, Zhe Qu, Jin Ge, Oliver G. Schmidt*

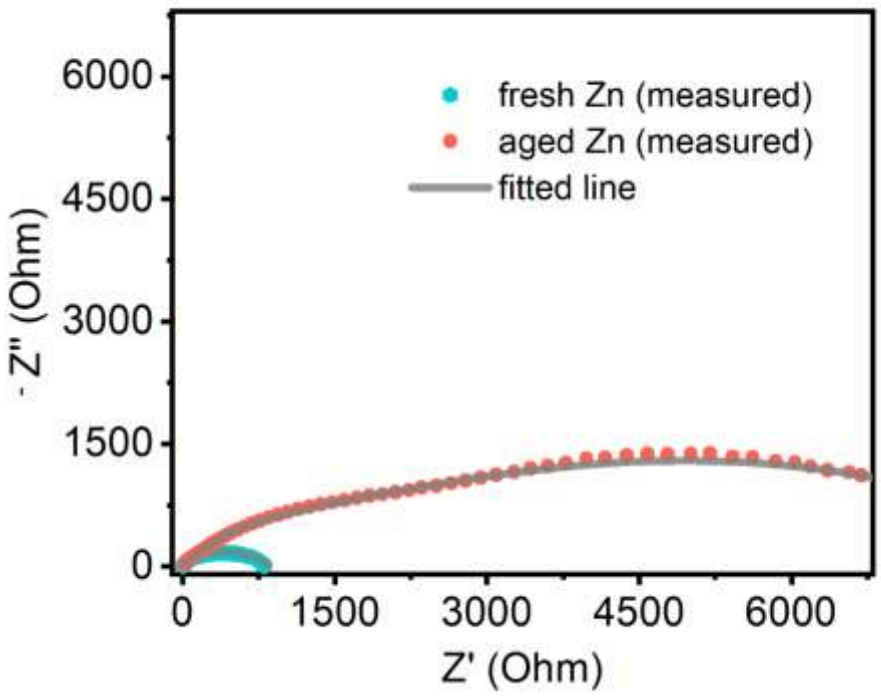

Figure S1. Nyquist plots and fitted results of a fresh Zn electrode and a Zn electrode immersed in 2 mol L^{-1} $ZnSO_4$ for 24 hours.

Table S1. Fitted parameters of the components in the equivalent circuit in Figure 1b.

	R_s (Ω)	R_{dl} (Ω)	Q_{dl} (n value)	R_{cl} (Ω)	Q_{cl} (n value)
Fresh Zn	8.7	7.2	1	845.1	0.49
Aged Zn	24.3	1.7×10^3	0.6	7.6×10^3	0.37

Figure S1 presents the Nyquist plots of the fresh and aged Zn electrodes in 2 mol L^{-1} electrolyte. The Nyquist plots are fitted by the equivalent circuit shown in Figure 1b. The fitted line and results are shown in Figure S1 and listed in Table S1. The aged Zn shows a sluggish ion transport as the n values of Q_{dl} and Q_{cl} decrease. The degradation is further proved by the dramatically increased of resistances, including system, double layer, and corrosion layer resistance. Both of the retarded ion transport and large resistances demonstrate the instability issue of Zn in a mildly acidic electrolyte.

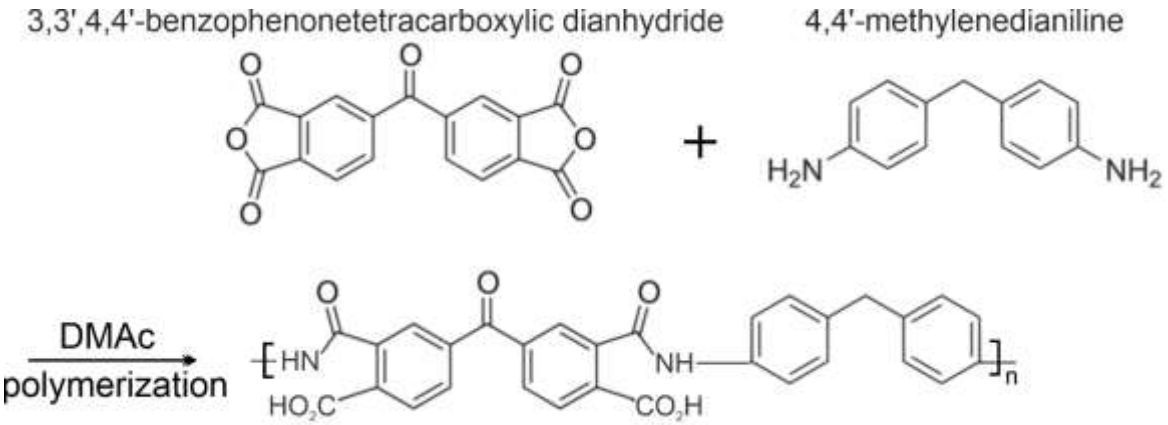

Figure S2. UV polymerization of the poly (amic acid).

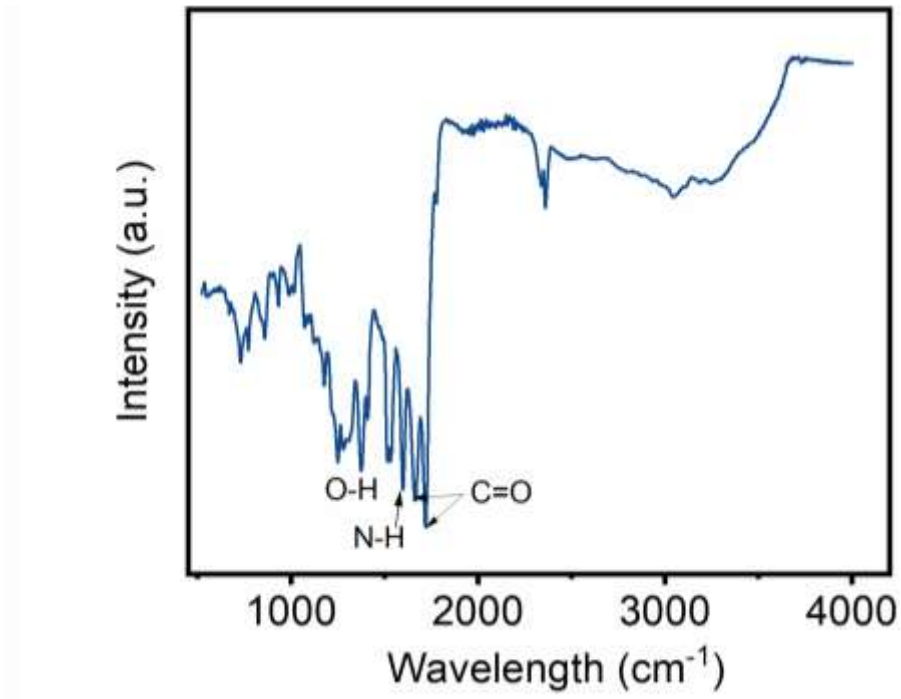

Figure S3. FTIR spectrum of the poly (amic acid).

Figure S2 shows the synthetic route to the poly (amic acid), which is produced by polymerizing 4,4'-methylenedianiline and 3,3',4,4'-benzophenonetetracarboxylic dianhydride under UV light. Figure S3 gives the FTIR spectrum of the poly (amic acid). The characteristic peaks of O-H stretching from the carboxyl group, N-H stretching from the amino group, and two different C=O stretching are observed, indicating the formation of the poly (amic acid). In comparison to the FTIR spectrum of the polyimide, the O-H, N-H, and carboxylic C=O stretching disappear.

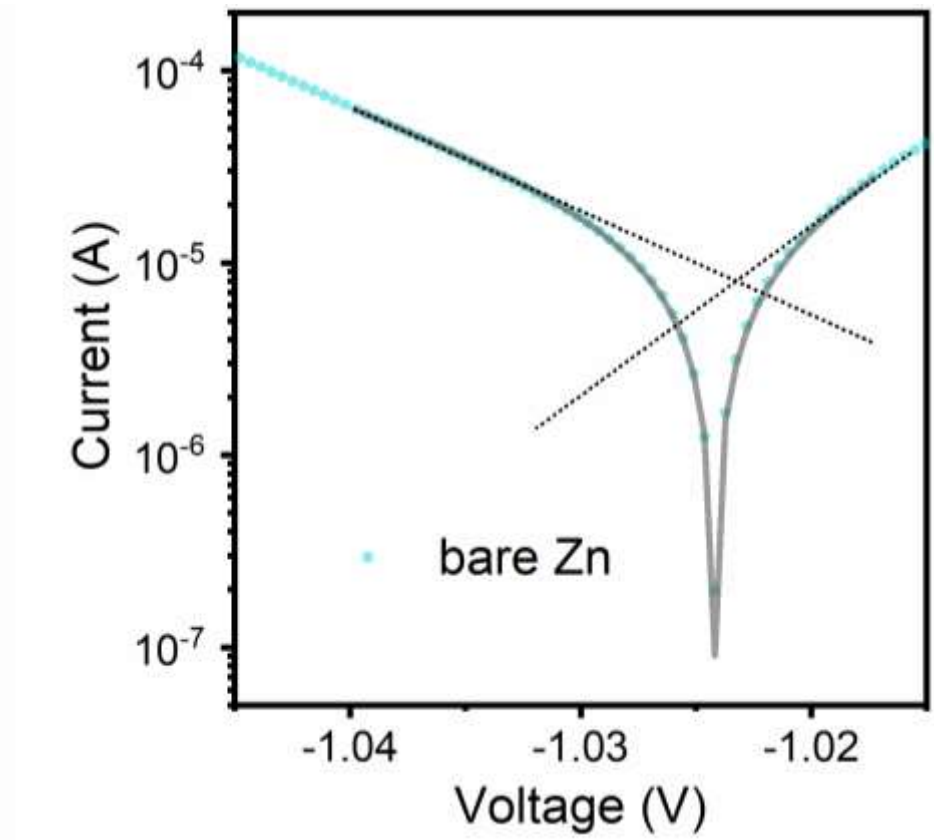

Figure S4. Linear polarization curve of the bare Zn at a sweep rate of 1 mV s^{-1} and the fitted result by Butler-Volmer equation.

Figure S4 gives the Tafel curve and Butler-Volmer fitted result of the bare Zn electrode. The corrosion current is calculated as 12 μA cm^{-2}. The corrosion potential is -1.02 V *vs.* SCE. The corrosion rate is as high as 0.35 mm per year, demonstrating that Zn is instable and can be easily corroded in 2 mol L^{-1} $ZnSO_4$ solution. At the microscale, the thickness of the Zn is usually controlled to sub-μm. In this case, the service time of a microbattery using Zn as the anode can hardly exceed one year.

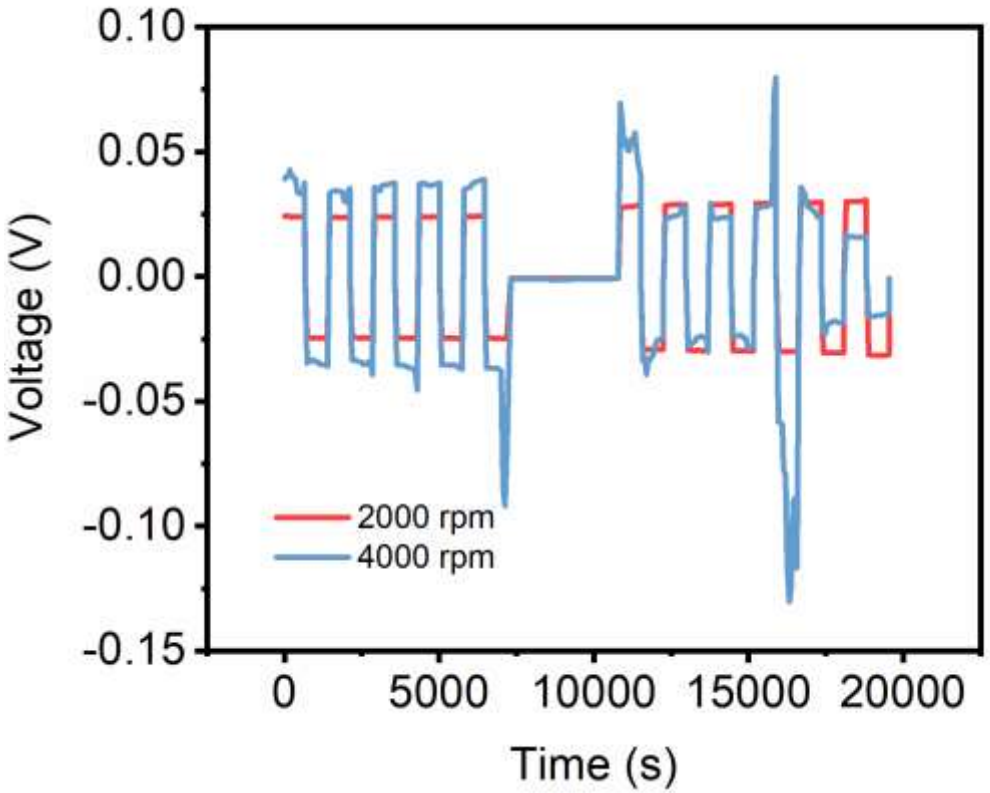

Figure S5. Galvanostatic charge/discharge profiles of piZn with the polyimide thickness of ~570 nm (2000 rpm) and ~ 380 nm (4000 rpm).

The sample with the polyimide thickness of ~380 nm fails in only five cycles as the severe fluctuation of overpotential is observed, especially after 1-hour rest period, indicating the polyimide is too thin to protect the Zn anode from corrosion.

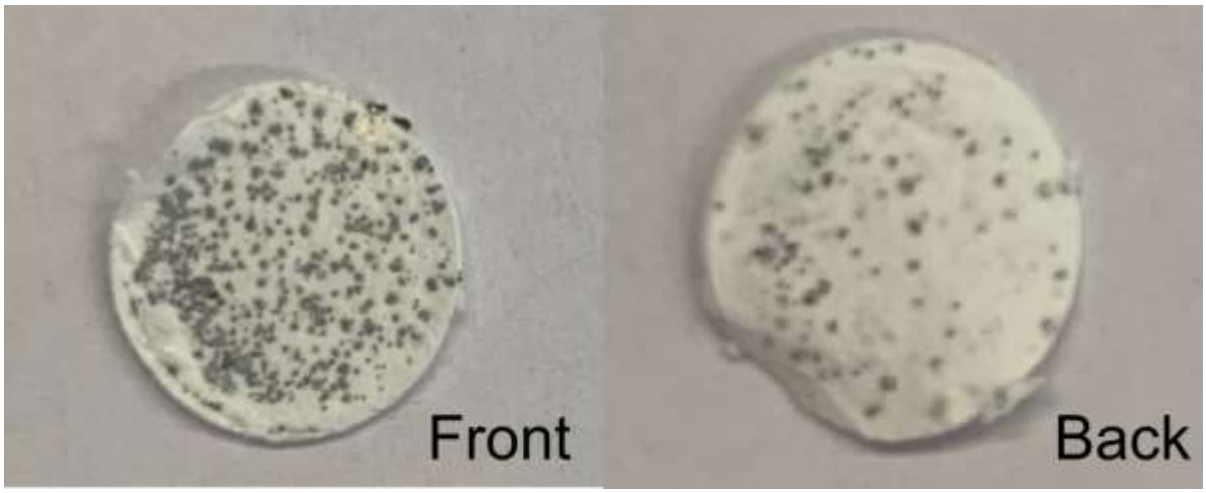

Figure S6. Images of the glass fiber separator of a Zn/Zn symmetrical cell after 500 galvanostatic charge/discharge cycles at 4 mA cm^{-2}.

Figure S5 shows the separator of a cycled Zn/Zn symmetrical cell. We can observe precipitated Zn on both sides of the separator, which leads to the short-cut of the cell and causes the failure.

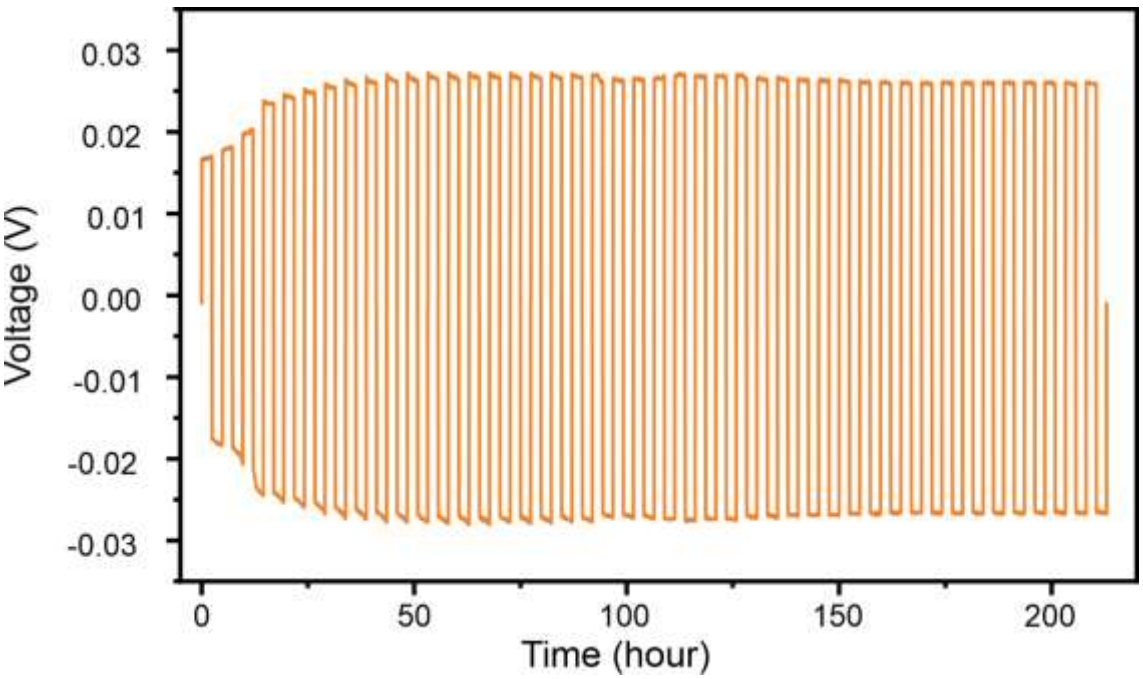

Figure S7. The galvanostatic charge/discharge profile of a piZn/piZn symmetrical cell with a DOD/SOC of 85%.

Figure S6 provides a stable galvanostatic charge/discharge profile with a deep charge/discharge depth (85%) of a piZn/piZn symmetrical cell. Accordingly, a high utilization of Zn can be accomplished, which will benefit the design of a high-performance microbattery.

Table S2. Comparison of various Zn stabilization strategies.

Strategy	Overpotential (mV)	Stability (h)	CE (%)	DOD (%)	Ref.
Polyamide	100 @ 0.5 mA/cm^2	8000	95.12	85	[1]
$CaCO_3$	40 mV @ 0.25 mA/cm^2	800	-	-	[2]
ZnS	50 mV @ 2 mA/cm^2	1100	99.2	-	[3]
Nafion	50 mV	80	-	-	[4]
Lignin@Nafion	15 mV @ 0.6 mA/cm^2	376	-	-	[5]
ZIF8	75 mV @ 2 mA/cm^2	200	>98	-	[6]
PEO	150 mV @ 1 mA/cm^2	1500	98.6		[7]
Supersaturated electrolyte	28 mV @ 0.3 mA/cm^2	3000	-	-	[8]
Triethyl Phosphate Electrolyte	50 mV @ 0.5 mA/cm^2	2000	99.68	-	[9]
acetamide and $Zn(TFSI)_2$	50 mV @ 0.1 mA/cm^2	1000	99.9	-	[10]
Polyimide	25 mV @ 4 mA/cm^2	300	99.5	85	This work

Note: CE: Coulombic efficiency; DOD: Depth of discharge/charge

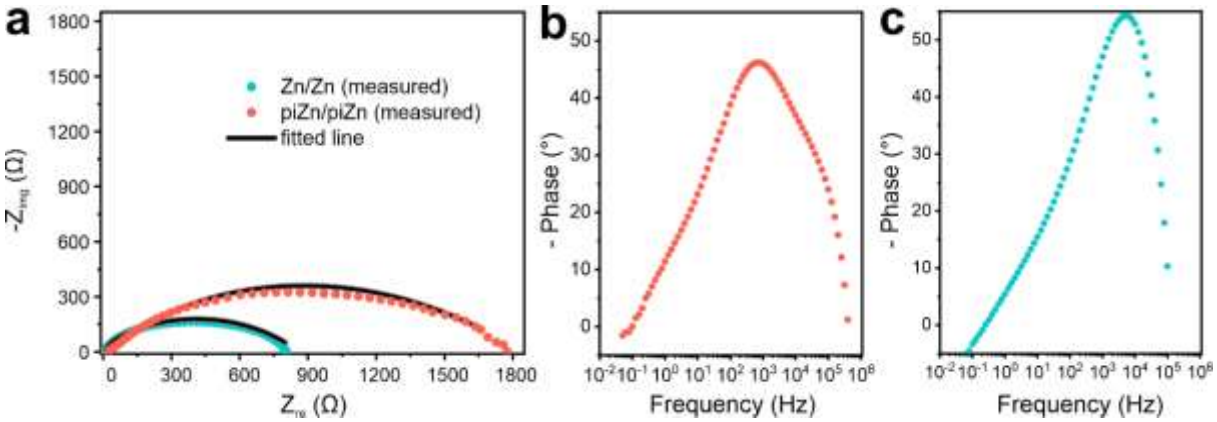

Figure S8. (a) Nyquist plots and fitted results of the fresh Zn electrode and piZn electrode. Bode plots of piZn/piZn (c) and Zn/Zn (c) cells.

Table S3. Fitted parameters of the components in the equivalent circuit in Figure 3a.

	R_s (Ω)	R_p (Ω)	Q_p (n value)	R_z (Ω)	Q_z (n value)
Zn/Zn	8.7	7.2	1	845.1	0.49
piZn/piZn	19.9	199.1	0.53	1.5×10^3	0

Figure S8a presents the Nyquist plots of the fresh Zn and piZn electrodes in 2 mol L^{-1} electrolyte. The Nyquist plots are fitted by the equivalent circuit shown in Figure 3a. The fitted line and results are shown in Figure S1 and listed in Table S3. The n values of Q_p and Q_z of the piZn electrode are different from those of the bare Zn electrode, hence predicting a different electrochemical behavior. The polyimide/electrolyte interface is diffusion controlled as confirmed by both a value of ~0.5 and a phase shift of ~45° in Figure S8b, indicating that ion can migrate into the polyimide layer. However, Zn/electrolyte interface is regarded as a resistor, implying the ionic conductivity of the polyimide layer is very low. By contrast, a short diffusion period is observed for bare Zn (Figure S8c), followed by transforming into a resistive behavior, indicating the passivation due to the corrosion.

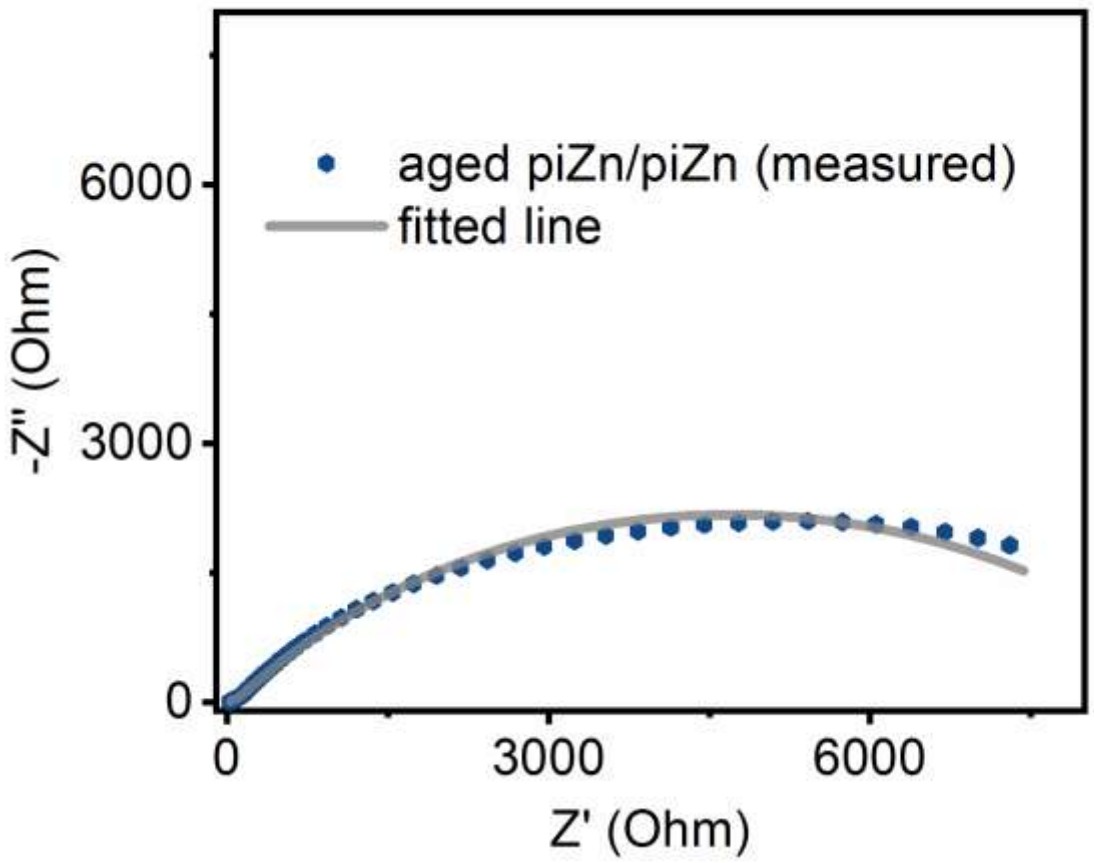

Figure S9. Nyquist plot of the aged Zn electrode.

After a 24-hour aging period, the electrochemical behavior remains same as the same equivalent circuit used in Figure 3a fits the measured data very well. The charge transfer resistance decreases from 199 to 42.5 Ω, demonstrating that the polyimide coating will slowly uptake Zn ions and form an ionic conductive interface. The interaction between Zn ions and polyimide in an aging test further confirms the formation of a polymeric zinc layer.

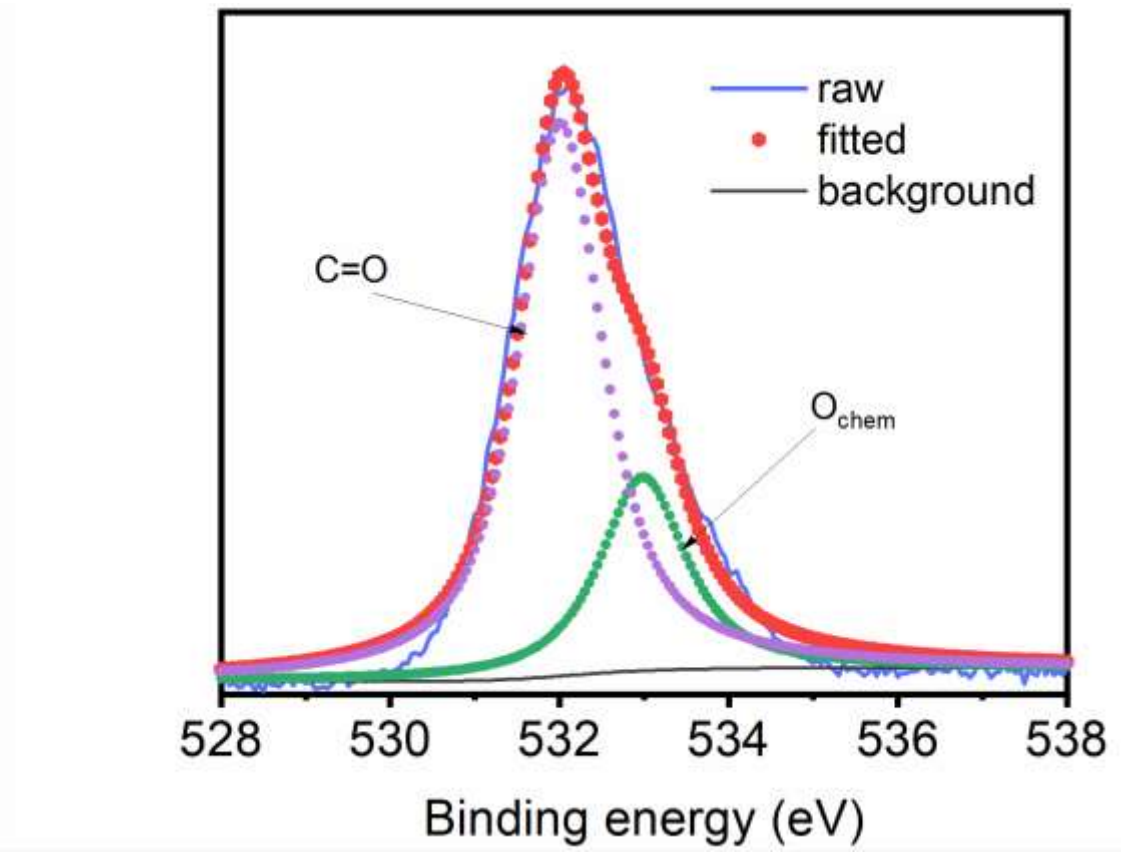

Figure S10. O 1s core level spectrum of the fresh piZn electrode.

Figure S10 gives the O 1s core level spectrum of the fresh piZn electrode. The spectrum is deconvolved into two species. A strong C=O bonding from the N-C=O group in the polyimide is observed. Besides, a small shoulder peak (O_{chem}) is associated with the interaction with the oxygen atoms and Zn^{2+} ions in the polyimide matrix. The intensity ratio between the C=O and O_{chem} is 0.35, indicating the strong interaction between the carbonyl oxygen atoms and cations resulting from the Lewis base feature of the polyimide and the large electron density of the Zn^{2+} ions. This unique feature benefits the formation of a Zn blanket to improve the reversibility of Zn chemistry.

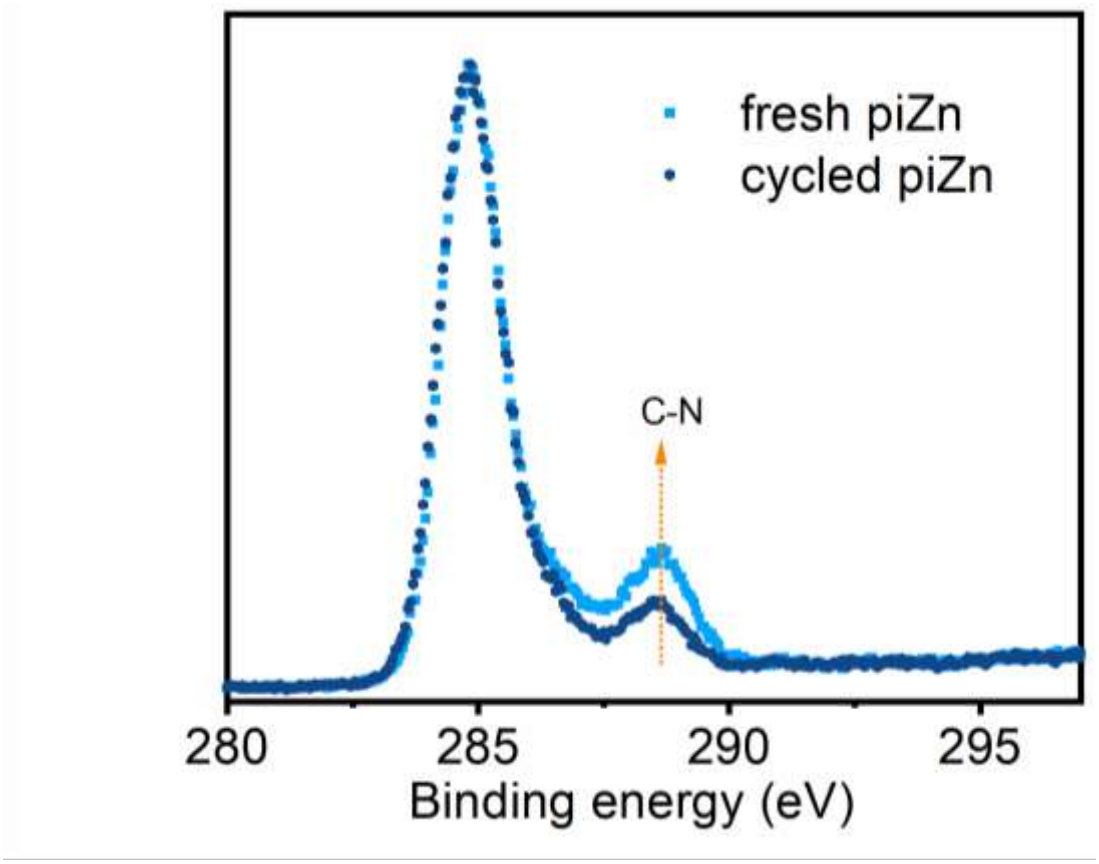

Figure S11. C 1s core level spectra of the fresh piZn and cycled piZn.

Figure S11 gives the C 1s core level spectrum of the fresh and cycled piZn electrodes. The peak centered at 285 eV is associated with the C-C and C=O bonds. The shoulder peak centered at 288.5 eV is attributed to the C-N bond. Upon cycling, we only observe that the C-N peak's intensity decreases, while the main peak remains identical. This evidence demonstrates that albeit the C-N bonds break over cycling, amino and carboxylic groups won't form.

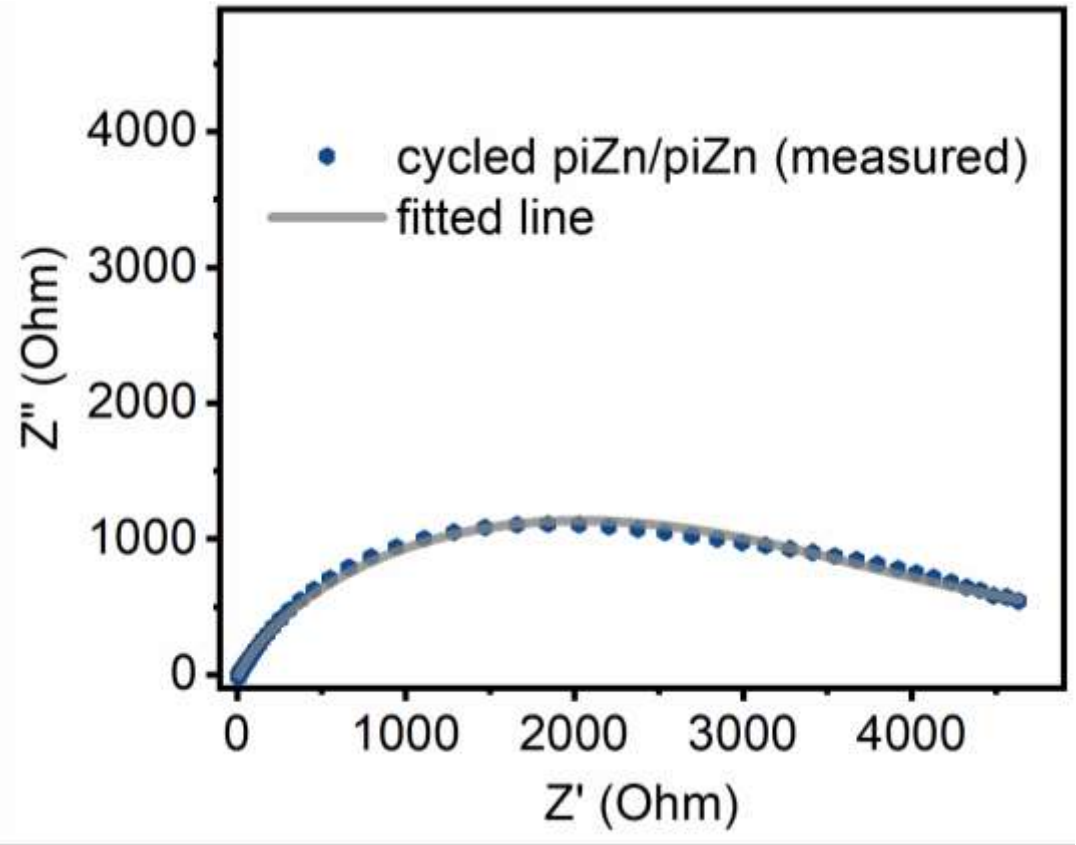

Figure S12. Nyquist plots and fitted results of the cycled piZn electrode.

Table S4. Fitted parameters of the components in the equivalent circuit in Figure 3a.

	R_s (Ω)	R_p (Ω)	Q_p (n value)	R_z (Ω)	Q_z (n value)
Cycled piZn	10.7	1.5×10^3	0.73	1.7×10^3	0.65

Figure S12 presents the Nyquist plots of the fresh Zn and piZn electrodes in 2 mol L^{-1} electrolyte. The Nyquist plots are fitted by the equivalent circuit shown in Figure 3a. The fitted line and results are shown in Figure S12 and listed in Table S4. In comparison to the fresh piZn, the n values of Q_p and Q_z increases, indicating an improved ion transport, which is confirmed by the activation process observed in the coulombic efficiency test and the increasing Zn transference number over cycling. All these results demonstrate a *in-situ* formed Zn blanket allowing for a highly reversible Zn chemistry.

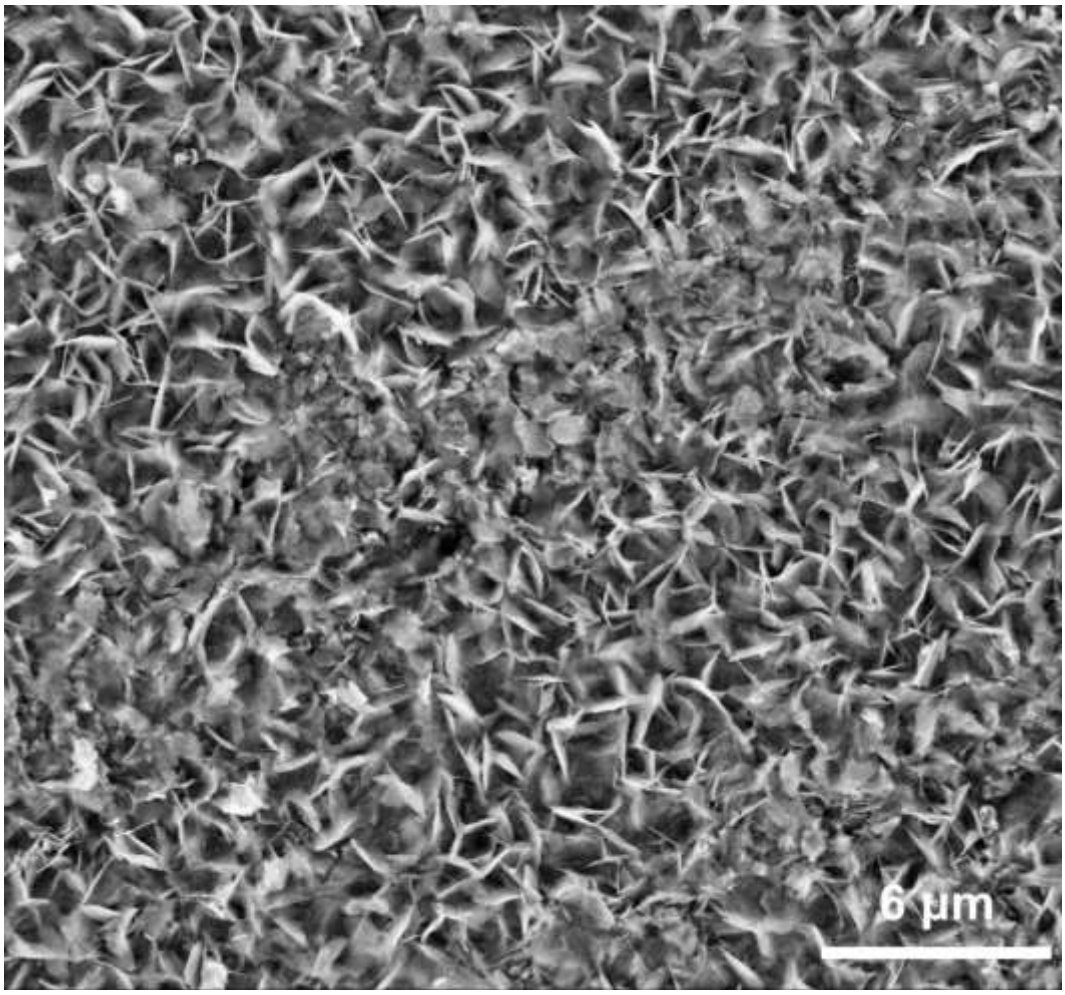

Figure S13. SEM image of the electrochemically deposited Zn in a microbattery, showing an assembly of Zn nanosheets.

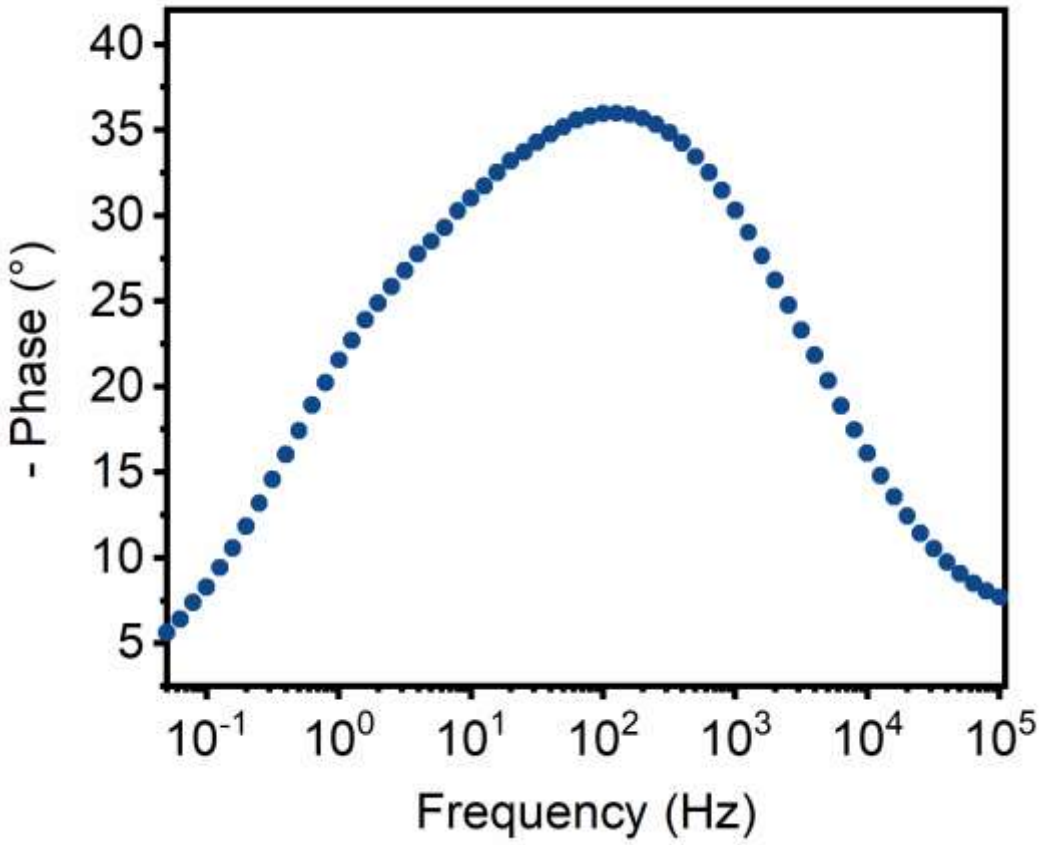

Figure S14. Bode plot of the piZn microanode.

Figure S15. Image of hydrogen generation and corrosion of the Zn microanode.

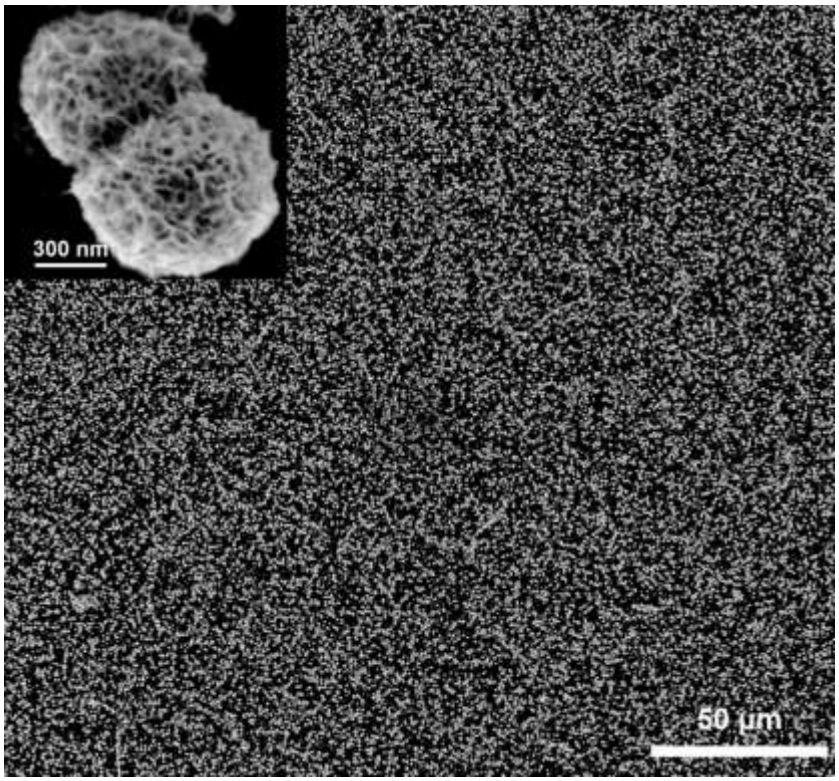

Figure S16. SEM image of the deposited MnO_2 in a microbattery, showing an assembly of MnO_2 porous spheres (inset).

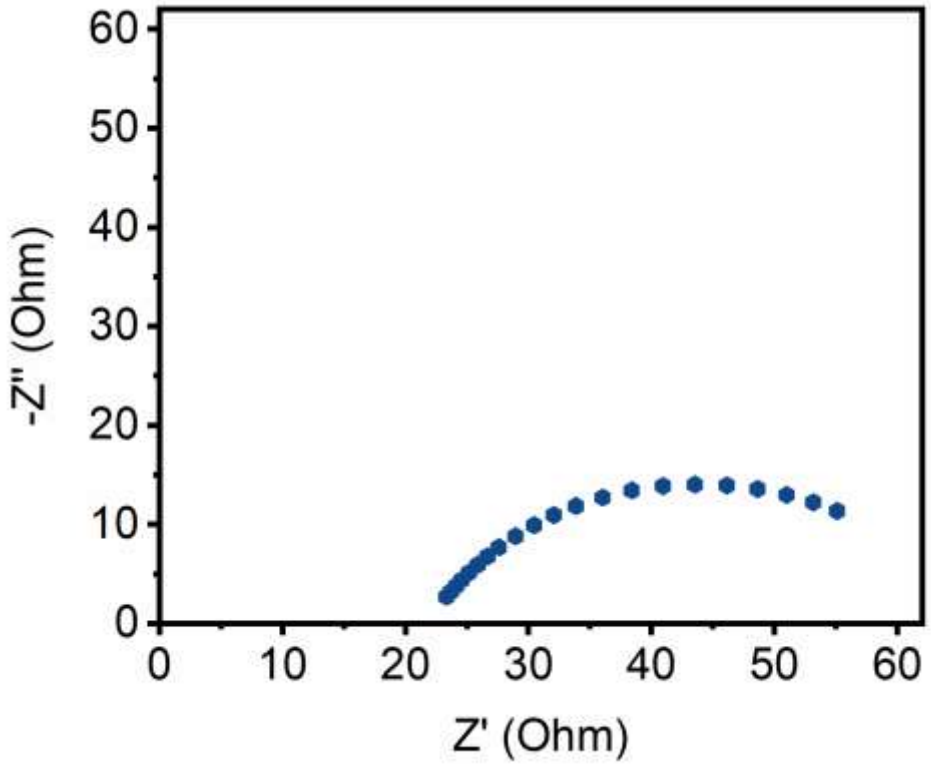

Figure S17. Nyquist plot of a piZn microanode with the PAAm electrolyte.

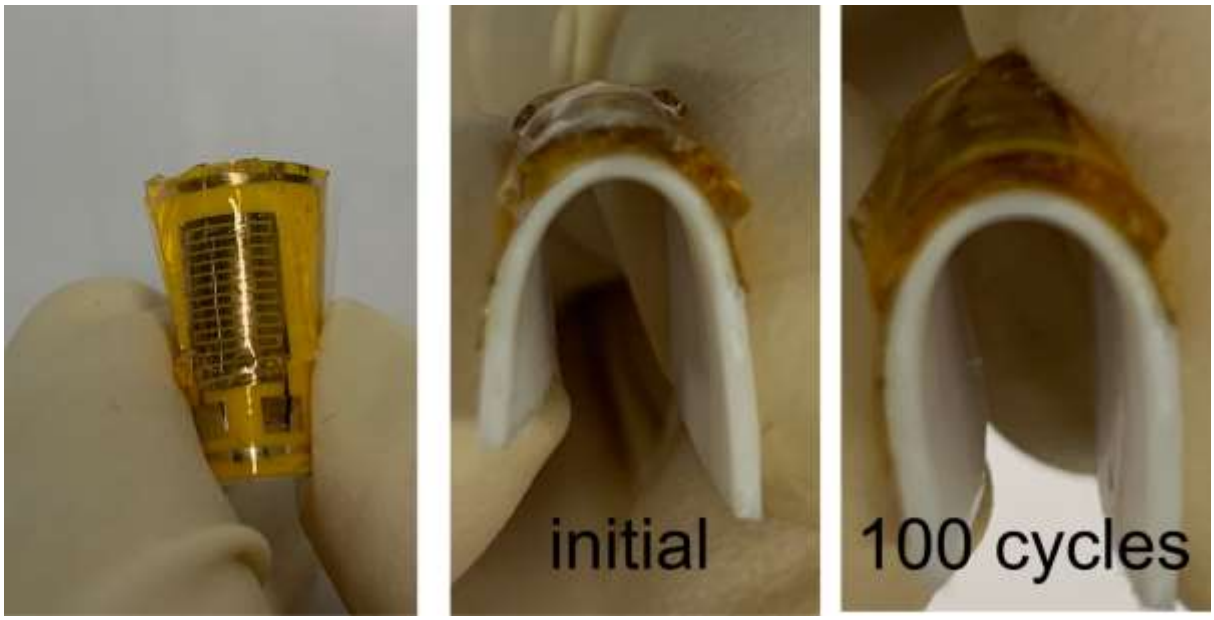

Figure S18. Images of PAAm on a skin-mountable microbattery and its adhesion over bending cycles.

References:

[1] Z. Zhao, J. Zhao, Z. Hu, J. Li, J. Li, Y. Zhang, C. Wang, G. Cui, *Energy Environ. Sci.* **2019**, *12*, 1938.

[2] L. Kang, M. Cui, F. Jiang, Y. Gao, H. Luo, J. Liu, W. Liang, C. Zhi, *Adv. Energy Mater.* **2018**, *8*, 1801090.

[3] J. Hao, B. Li, X. Li, X. Zeng, S. Zhang, F. Yang, S. Liu, D. Li, C. Wu, Z. Guo, *Adv. Mater.* **2020**, *32*, 2003021.

[4] M. Ghosh, V. Vijayakumar, B. Anothumakkool, S. Kurungot, *ACS Sustain. Chem. Eng.* **2020**, *8*, 5040.

[5] D. Yuan, W. Manalastas, L. Zhang, J. J. Chan, S. Meng, Y. Chen, M. Srinivasan, *ChemSusChem* **2019**, *12*, 4889.

[6] Z. Wang, J. Huang, Z. Guo, X. Dong, Y. Liu, Y. Wang, Y. Xia, *Joule* **2019**, *3*, 1289.

[7] Y. Jin, K. S. Han, Y. Shao, M. L. Sushko, J. Xiao, H. Pan, J. Liu, *Adv. Funct. Mater.* **2020**, 2003932.

[8] H. Yang, Z. Chang, Y. Qiao, H. Deng, X. Mu, P. He, H. Zhou, *Angew. Chem. Int. Edit.* **2020**, *59*, 9377.

[9] A. Naveed, H. Yang, J. Yang, Y. Nuli, J. Wang, *Angew. Chem. Int. Edit.* **2019**, *58*, 2760.

[10] H. Qiu, X. Du, J. Zhao, Y. Wang, J. Ju, Z. Chen, Z. Hu, D. Yan, X. Zhou, G. Cui, *Nat. Commun.* **2019**, *10*, 5374.